RSC Advances

ROYAL SOCIETY OF CHEMISTRY

www.rsc.org/advances

Highly efficient NIR to visible upconversion in ZnO:Er,Yb thin film deposited by AACVD atmospheric pressure process

R. Elleuch*[,a], R. Salhi[b], J.-L. Deschanvres[c] and R. Maalej[a]

[a]Laboratoire Géoressouces, Matériaux, Environnement et Changements Globaux, Faculté des Sciences de Sfax, Université de Sfax, 3018 Sfax, Tunisia

[b]Laboratoire de chimie industrielle, Ecole Nationale d'ingénieurs de Sfax, Université de Sfax, 3018 Sfax, Tunisia

[c]Laboratoire des Matériaux et du Génie Physique, 3 Parvis Louis Néel, BP 257, 38016 Grenoble, France

E-mail : ridhaelleuch@yahoo.fr

The table of contents entry (TOC)

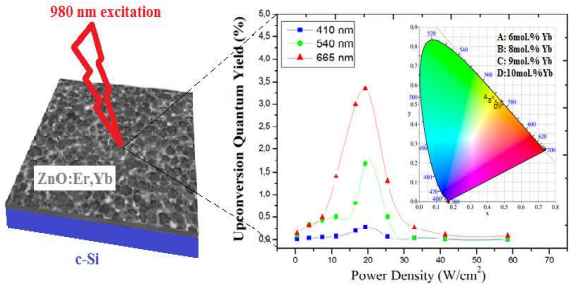

ZnO:Er,Yb hexagonal wurtzite phased structure thin film with high efficient NIR to visible upconversion emissions

ABSTRACT: ZnO:Er^{3+},Yb^{3+} thin films with hexagonal wurtzite structure were successfully deposited on Si (111) substrates at 430°C by aerosol-assisted chemical vapor deposition (AACVD) atmospheric pressure process. Films were deposited with fixed 3 mol.% Erbium concentration and various Ytterbium concentrations of 6, 8, 9 and 10 mol.%. The annealing treatment at 1000°C was found to enhance the crystallinity and the upconversion (UC) emission of the films. UC emissions were investigated under 980 nm excitation, and the ZnO:Er^{3+},Yb^{3+} films exhibited the intense red 665 nm upconverted emissions of Er^{3+} ions originating from an efficient Yb-Er energy transfer process. The absolute upconversion Quantum Yield (UC-QY) of each film was measured for the UC emissions centered at 410, 540 and 665 nm at varying excitation power densities. UC-QY analysis has revealed that ZnO: 3mol.%Er, 9 mol.% Yb thin film possess the highest total quantum yield of 5.59±0.1% with a power density of 19.3±3 W/cm^2. These results show that this film is promising as an efficient upconversion layer suitable for many photonic applications.

1.INTRODUCTION

Up-conversion (UC) materials such as nanoparticles, polymer and glass materials doped with rare-earth (RE) ions have numerous potential applications, including 3-D displays, UC lasers, optical temperature sensing, biological labels, wastewater and photodynamic therapy. [1-7] Near infrared (NIR) to visible nanocrystals upconverters have significant potential in biological labels because NIR excitation penetrates deeply into biological tissue and generates virtually no unwanted fluorescence background signal. Moreover, UC nanocrystals can eliminate any autofluorescence from biosamples, minimize photodamage, and increase the penetration depth.[8] In another hand, thin UC films are usually required when they are applied as spectral converters in photovoltaic (PV) cells,[9] multilayer optical storage disks[10] and luminescent screens for optically written displays.[11] To date, different UC thin films are made from RE activated fluorides or oxides. In addition, transparent conducting oxides (TCO) have an immense applications in optoelectronic devices such as flat panels, solar cells and light emitting diodes (LEDs).[12,13] Recently, TCO Zinc oxide thin film material has become an interesting scope of research in various applications such as antireflective coating[14] and transparent electrodes in solar cells.[15] Doping high refractive index materials with RE ions is one of the most promising approaches, which has not been investigated yet. The optical properties of ZnO, in particular, have been attractive because this material has a narrower band gap (3.3 eV) than that of the widely studied GaN and AlN, whilst maintaining a suitable energetic band.[16] Compared with other optical materials, ZnO has superior qualities such as high refractive index[17] (~2) and excellent physical and chemical stability.[18] Numerous techniques were used for the growth of the RE-doped ZnO thin films such as implantation,[19] RF magnetron sputtering[20] and electrodeposition method.[21] Aerosol-assisted chemical vapor deposition (AACVD) at atmospheric pressure process presents some key advantages,

including a mass production with large area, a wider choice and availability of precursors, high CVD quality products and stoichiometric control of the dopants.[17,22,23]

On the other hand, it is well known that the local symmetry restriction around rare earth ions leads to a relative weak UC emitted from a material doped only with Er^{3+}. Fortunately, UC emission intensities can be enhanced when Yb^{3+} ions are co-doped with Er^{3+}. Yb^{3+} ion (with only emission at 1000 nm from the $^2F_{5/2} \rightarrow {}^2F_{7/2}$ transition) has a much greater absorption cross section and a broader absorption band in comparison with the Er^{3+} ion under the excitation of 980 nm photons, leading to a very high Yb-Er energy transfer efficiency.[24] In particular, Er^{3+} and Yb^{3+} ions are efficient UC couple when the Er^{3+} ion is an excellent candidate for UC as its metastable levels $^4I_{11/2}$ which can be conveniently populated.[25]

The key figure of merit for the upconversion materials is the determination of the upconversion quantum yield (QY) of its UC process. Although several research works have been reported on the optimization of the RE doping ions in the host matrix to achieve the highest UC luminescence. But until now, the literature is lacking comprehensive investigations on the optimum doping level of the RE ions. Kano et al. reported an investigation of β-$NaYF_4$ samples codoped with Yb^{3+} and Er^{3+} doping concentrations.[26] For a fixed Yb^{3+} doping of 39%, an optimum Er^{3+} doping of approximately 3% was optimized. Another investigation on the β-$NaYF_4$, codoping with 2% Er^{3+} and 18−20% Yb^{3+} are used to the optimization of the RE doping for high QY value.[27] However, it is not clear whether this is the optimum combination of the highest UC-QY, and consequently the brightest possible response (luminescence) of the upconverter. It is worthy to note that obtaining a high QYs at lower excitation power densities make the materials suitable for Si solar cells applications.[28]

The biggest hindrance of using UC thin film is its low luminescent efficiency compared to those in powder and bulk counterparts. Thus, there have been enormous efforts to improve

luminescent efficiency in semiconductor thin film. This framework reports on the enhancement of the UC emissions of Er,Yb:ZnO thin films on Si (111) substrates with large surface of (3 inches x 3 inches) deposited by AACVD atmospheric pressure process. Optimization of the Yb concentrations and deposition conditions effects on the crystallinity, UC emissions and UC-QY of the films were investigated in details.

2. EXPERIMENTAL SECTION

2.1. **Synthesis.**

Double (Er^{3+}/ Yb^{3+}) ion/ions doped ZnO thin films were deposited on Si (111) substrates in a hot walled reactor using a liquid source AACVD process described elsewhere.[29] The stoichiometric amounts of high-purity grade zinc acetate dihydrate ($C_4H_6O_4Zn\cdot 2H_2O$), Erbium (III) tris(2,2,6,6-tetramethyl-3,5-heptadionate) ($Er(TMHD)_3$)) and Ytterbium (III) tris(2,2,6,6-tetramethyl-3,5-heptadionate) ($Yb(TMHD)_3$)) (STREM chemicals society) chemicals were used and dissolved in a mixing of 460 ml methanol and 40 ml butanol solvent with 0.05 M total concentration. These chemicals were selected for their non-toxicity, good stability at room temperature, easy handling and high volatility. $Er(TMHD)_3$ molar percentage was fixed at 3 mol.%, and various $Yb(TMHD)_3$ molar percentages were 6, 8, 9 and 10 mol.%. The homogeneous chemical solutions were then heated for 1h on a hot plate with magnetic stirring and their temperatures were kept at 80 °C.

2.2. **Thin film Deposition**

In the first deposition steps, Si (111) substrates were maintained at 430°C for 30 min using an atmospheric air environment. The solutions were kept in the flask which is fixed on a flat ultrasonic piezoelectric transducer to create the aerosol. Tailored aerosol flow at 2 $cm^3.min^{-1}$ was carried to the heated substrate using air as carrier gas at a flow rate of 4 $l.min^{-1}$.

The ZnO:Er,Yb thin films were obtained by the thermal decomposition of the monodisperse droplet sized of 2–4 μm on the top of the Si surface substrate. A uniform delivery rate of the precursor aerosol to the heated Si substrate resulted in a good uniformity of the deposited films.

2.3. Characterization

The Field Emission Scanning Electron Microscope (FE-SEM) images were obtained on an FEI Quanta FEG 250 using an accelerating voltage of 15 keV with 10^{-4} Pa pressure. The film thickness was measured by an ellipsometer Gaertner L116B using a 632.8 nm wavelength and normal incidence. Films structures were investigated by a diffractometer Siemens D500 with Cu Kα radiation in θ/2θ scan. Photoluminescence (PL) spectra were recorded under 488 nm excitation using a Jobin–Yvon Horiba LabRam spectrometer equipped with liquid nitrogen cooled CCD detector and with 11 mW of excitation power. Laser diode with 980 nm was used as excitation and the UC spectra were recorded in [500-850 nm] with a Jobin-Yvin U1000 spectrometer. The UC-QY of the films were measured using a Edinburgh Instruments (FLS920) spectrofluorometer equipped with an integrating sphere (Jobin-Yvon) equipped with a Hamamatsu (R-5587) liquid nitrogen cooled 980 nm phototube. Monochromatic excitation light was selected from a supercontinuum laser (Fianium SC400 6W) with a double monochromator. 5 mm diameter of the ZnO:Er,Yb films were placed at the focal point of the excitation light. The error involved in the UC-QY measurements is about 5 % relative. Only the $^4I_{11/2} \rightarrow {}^4I_{15/2}$ transition was considered for the UC-QY measurements. To eliminate any contributions of the ZnO host matrix to the emission and the scatter spectra, undoped ZnO film was used as a reference samples and placed in a dish made of synthetic quartz which suppress luminescence. To determine the dependence of the UC-QY on the

pump power, QY and power density were recorded using various filters with the same beam area for all the measurements.

3. RESULTS AND DISCUSSION

3.1. Morphology observation

The FESEM images shown in Figure 1 present the surface morphologies of as-deposited films grown by AACVD liquid source process. The ZnO:Er/Yb films with fixed 3 mol.% Er deposited at 430°C for 30 min reveal a growth rate in the range of 620-640 nm/h with film thicknesses of 310, 314, 316 and 320 nm corresponding to 6, 8, 9 and 10 mol.% Yb, respectively. It is observed that the surfaces are composed of nanograins stagged on the top of the films. In the deposition process, the precursor droplets are thermally dissociated, leading to an aggregation of nanograins on the surface with the average diameter of about 120 nm. It is found that all the films have an identical surface morphology with a fairly homogeneous nanograins distribution. It is noted that the grown mode of ZnO:Er,Yb films by AACVD process is a Volmer-Weber type film growth, when the nanograins were assumed as a 3D-island growth mode resulting from the nucleation of ZnO:Er/Yb onto the Si substrate surface.[17, 30]

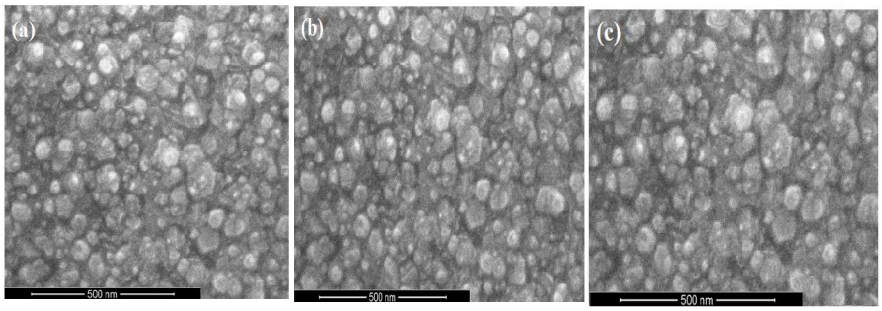

Figure 1. FESEM images of ZnO:Er,Yb thin films deposited by AACVD process on Si(111) substrates with various Yb ion concentrations of: (a) 8 mol.%, (b) 9 mol.% and (c) 10 mol.%.

3.2. Crystal structure analysis

Figure 2 shows the x-ray diffraction (XRD) patterns of the as-deposited ZnO: 3mol.%Er,9mol.%Yb thin film deposited at 430°C by AACVD process, indicating that this film is polycrystalline in nature. It is observed that all the as-deposited films have the same XRD patterns (not shown). Indeed, all the diffraction peaks can be readily indexed to the pure ZnO wurtzite hexagonal phase according to the JCPDS file no. 36–1451. Moreover, no additional peaks of other phases are observed, which indicates that the $Er^{3+}$and Yb^{3+}ions are well incorporated into the ZnO host.[29,30]

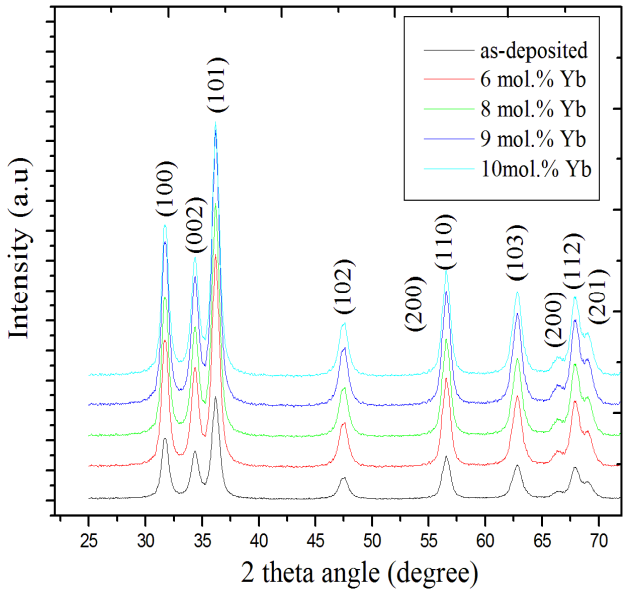

Figure 2. XRD patterns of the as-deposited (at 430°C) and annealed (at 1000°C) ZnO:Er,Yb films with various Yb concentrations doping.

It is well known that after deposition of films using β- dictonate precursors and alcohol solvents with AACVD process, the hydroxyl -OH groups and organic residua with some contaminations like C=C and C=O are still remain on the top of the films surface and their presence eradicate the luminescence of rare earth ions.[17,29,30] Hence, post annealing at 1000 °C in air atmosphere is an indispensable treatment for the disappearance of the hydroxyl and

organic contaminations and the enhancement of both crystallinity and the optical response of the films.[17, 29, 30]

After annealing in air atmosphere for 1h at 1000°C, the XRD patterns of ZnO:Er,Yb thin films were measured as shown in Figure 2. Following this treatment, the XRD patterns of the annealed films show a hexagonal phased ZnO structure similar to the as-deposited ones. These observed diffraction peaks are more intense than those of as-deposited ones, indicating an improvement in the crystalline structure.[17,29,30] Actually, the films show a structural stability and a more ordered crystalline structure with annealing treatments in air atmosphere, originating from the reorganization of the atoms, reduction of the defect density and the establishment of the proper stoichiometry.[17,30,31] It is also found that the hexagonal ZnO structure for the annealed films is not altered by the presence of Yb^{3+} and Er^{3+} ions. Indeed, no other phase of Yb_2O_3 and/or Er_2O_3 appeared in XRD patterns, indicating a good incorporation of the dopant ions in the matrix by the substitution of Zn^{2+} ions.[17]

3.3. Photoluminescence emission

As shown in Figure 3, under 488 nm excitation wavelengths, the PL spectra of the as-deposited and annealed ZnO:3mol.%Er, 9mol.%Yb film at 1000°C film were recorded at room temperature. Indeed, very weak PL emissions of the as-deposited films are detected, and only the annealed ones have strong PL emissions. It is to be noted that these observed luminescence bands are attributed to the 4f–4f transitions of Er^{3+} incorporated in ZnO matrix since Yb^{3+} have only one emission at 1000 nm. These PL emissions intensities are distinctly enhanced for the film annealed at 1000 °C by 25 times higher than the as-deposited one. The observed green luminescence occurring from 520 nm to 535 nm is attributed to $^2H_{11/2} \rightarrow {}^4I_{15/2}$ transitions and the second emission ranging from 540 to 570 nm is ascribed to $^4S_{3/2} \rightarrow {}^4I_{15/2}$ transitions. The red emission occurring from 645 to 685 nm is associated with the $^4F_{9/2} \rightarrow {}^4I_{15/2}$

transition of Er^{3+} ions.[31] We can see that the green emissions are more intense than the red ones, which is in accordance with the obtained results in our previous work reported on Er:ZnO thin films. Moreover, this study was also reported to check the incorporation of the RE ions within the host. The well and resolved PL spectrum from the ZnO: 3mol.% Er, 9mol.% Yb film deposited at 430°C and annealed at 1000°C is obtained when Er and Yb ions occupy C_{4V} site symmetry.[17,30,31]

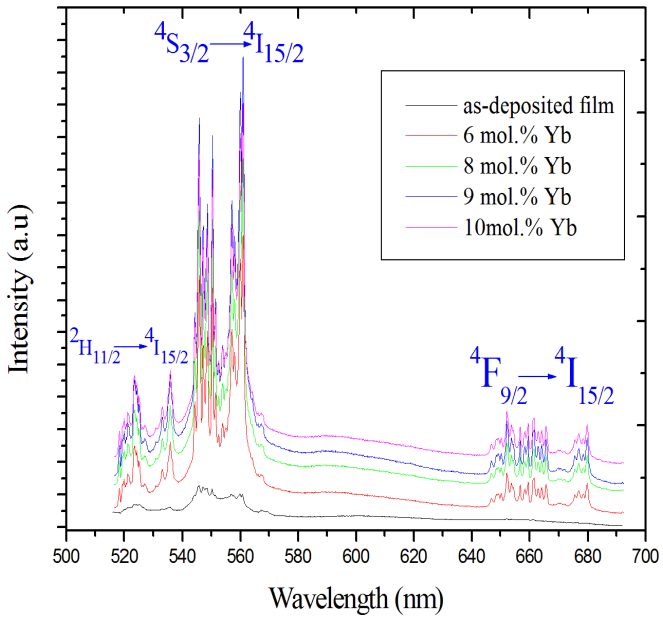

Figure 3. Room temperature PL emissions of ZnO:Er,Yb thin films annealed at 1000°C under 488 nm excitation with 11 mW excitation power. Observed PL emissions are attributed to Er^{3+} ions only.

3.4. Upconversion emission

Figure 4a shows the room temperature upconversion emissions of the annealed ZnO:Er/Yb films at 1000°C under the direct excitation photon at 980 nm. It is seen that the observed optical emissions are assigned to the intra 4f transitions of the Er^{3+} ions. The UC emissions spectra exhibit two weak ultraviolet (UV) and green emissions, and also a strong red one. The observed UV 410 nm emission is associated with the $^2H_{9/2} \rightarrow {}^4I_{15/2}$ transition. The green bands

centered at 525 and 555 nm are assigned to the $^2H_{11/2} \rightarrow {}^4I_{15/2}$ and $^4S_{3/2} \rightarrow {}^4I_{15/2}$ transitions, respectively. The strong red emission band centered at 665 nm is ascribed to the $^4F_{9/2} \rightarrow {}^4I_{15/2}$ transition. It is noted that the strongest red emission intensity is attributed to the film doped with 9 mol.% Yb concentration compared to the other films. These intense and well resolved emission take place, leading to the optical active center of Er^{3+}/Yb^{3+} in the ZnO lattice with a local structure similar to that of the ErO_6 unit.[31] After annealing, the local structure around Er/Yb probably forms a similar pseudo-octahedron with C_{4v} point structure by the diffusion of excess Oxygen O, leading to higher PL intensity.[17,29,31] The most resolved and strongest emissions were detected for the film having 9 mol.% Yb content indicating a maximum doping concentration of the Er/Yb incorporated in the matrix. The Yb concentration dependence upconversion emissions of the annealed ZnO:Er,Yb thin films are investigated and it is concluded that, with the increase of Yb^{3+} concentration from 6 to 10 mol.%, the green emission intensity decreases remarkably while the red emission intensity increase. This result is in good agreement with that observed by Vetrone et al. in Y_2O_3:Er,Yb nanocrystals.[32] Therefore, it is possible to tune the emission color of the annealed ZnO:Er,Yb thin films by varying the Yb^{3+} concentration. The color chromaticity coordinates of the annealed ZnO:Er,Yb films are estimated using the commission of Internationale de l'Eclairage (CIE) 1931 color matching functions, and are represented in Figure 4b. Under 980 nm, the color chromaticity coordinates were calculated and found to be A(x=0.428 y=0.542), B(x=0.446,y=0.527), C(x=0.466,y=0.518) and D(x=0.573 , y=0.486) for Yb concentration of 6, 8, 9 and 10 mol.%, respectively. It is observed that, with increasing Yb^{3+} content, the emission color changes gradually from yellow to orange.

It is worthy to note that Er and Yb show two basic population mechanisms which can be involved in the upconversion process, namely energy transfer (ET) upconversion and excited

state absorption (ESA).[33] Their possible schematic diagram is shown in Figure 4c. Under the 980 nm excitation wavelength, the absorption transition between the ground state $^4I_{15/2}$ and the excited level $^4I_{11/2}$ (GSA) was established.[33] Besides, the same wavelength excites Er ions from the $^4I_{11/2}$ to $^4F_{7/2}$ level (ESA process). On the other hand, the Er^{3+} ion can be excited from the $^4I_{15/2}$ to $^4I_{11/2}$ level by the general multiphoton processes through the ground state absorption and the energy transfer from the excited Yb^{3+} ions $^2F_{5/2}$ level and presented in the following process:

$$^4I_{15/2}\,(Er) + {}^2F_{5/2}\,(Yb) \rightarrow {}^4I_{11/2}\,(Er) + {}^2F_{7/2}\,(Yb)$$

These energy transfer mechanism can dominate the UC emission process when the Yb^{3+} ions have a much larger absorption cross section then that of the Er^{3+} ions around 980 nm. Accordingly, the Er^{3+} ions were excited to the $^4I_{11/2}$ level in the first step by an energy transfer process from the excited Yb^{3+} ions $^2F_{5/2}$ level, and then the electrons in the $^4I_{11/2}$ level were excited to the $^4F_{7/2}$ level by the Er^{3+}/Yb^{3+} energy transfer or the ESA process. After that, a multiphonon relaxation was established, and the electrons were transited to the emitted $^2H_{11/2}$ and $^4S_{3/2}$levels and then de-excited to the $^4I_{15/2}$ leading to the green emissions. At the same time, the electrons in the $^4I_{11/2}$ excited state can decay nonradiatively to the $^4I_{13/2}$ state, and then transit to the $^4F_{9/2}$ level by energy transfer process from the excited Yb^{3+} ions $^2F_{5/2}$ level. Accordingly, the Er^{3+} ions electrons transit to $^4I_{15/2}$ and emit $^4F_{9/2}\rightarrow{}^4I_{15/2}$ red emission band. Another Er-Yb energy transfer mechanism can be established through the following process:

$$^4G_{11/2}\,(Er) + {}^2F_{7/2}\,(Yb) \rightarrow {}^4F_{9/2}\,(Er) + {}^2F_{5/2}\,(Yb)$$

As shown in this process, the electrons localized at the $^4S_{3/2}$ level can absorb another photon and transit to the $^2K_{15/2}$ level. Then, after a nonradiative decay to the $^4G_{11/2}$ state, the electrons can populate the $^4F_{9/2}$ state by energy transfer process from Yb^{3+} ions $^2F_{5/2}\rightarrow{}^2F_{7/2}$ transition. It

is concluded that the $^4F_{9/2}$ level was largely populated leading to the enhancement of the red emission with the increase of the Yb concentration. This is due to the decrease of the inter-atomic distance between the Yb^{3+} and Er^{3+} ions, thus facilitating the back energy transfer process ensured by the $^4G_{11/2}$ Er^{3+} and $^2F_{5/2}$ Yb^{3+} levels as described above. In conclusion, the cited energy transfer process suppresses the population of the $^2H_{11/2}$ and $^4S_{3/2}$ levels, leading to the decrease of the green emission and the enhancement of red emission.[34]

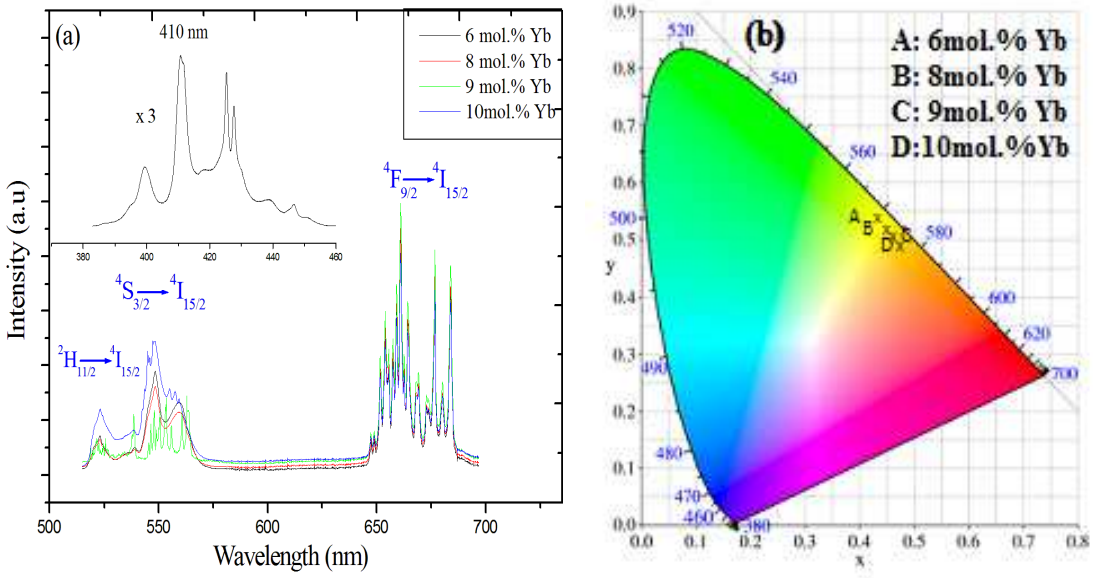

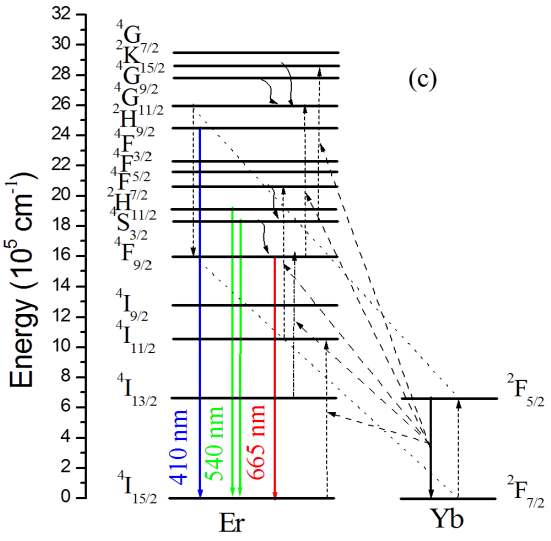

Figure 4. (a) Room temperature upconversion emissions of ZnO:Er,Yb annealed films under 980 nm excitation. (b) Energy level diagram of Er^{3+}/Yb^{3+} system codoped ZnO thin film showing possible excitation and de-excitation mechanism at 980 nm excitation. (c) Energy level diagrams of Yb^{3+} and Er^{3+}, and their possible UC processes.

3.5. Upconversion quantum yield

To accurately compare the optical properties of the present upconversion ZnO:Er,Yb thin films with those in literature, the quantum yield of the upconversion process was measured for the as-deposited and annealed films. The quantum yield is calculated using the following equation:[27]

$$\mathrm{QY} = \frac{E_{emission}}{E_{ref} - E_{sample}}$$

where, $E_{emission}$ is the integrated red, green or UV emission peaks, giving the number of photons emitted, E_{ref} is the integrated laser peak after absorption and scattering from an undoped ZnO reference and E_{sample} is the integrated laser peak of the sample itself, with their difference giving the number of photons absorbed. Theoretically, the upconversion from NIR to UV, green or red emissions requires two absorbed photons for each emitted photon, then the quantum yield will range from 0 to 50%. To obtain precise value of the quantum yield, measurements are in heavy dependence on various factors, such as the excitation power density, temperature of the sample and the reflectivity of the sample holder. For each QY measurement, an undoped ZnO reference film was used in an exactly similar way to most closely reproduce the scattering of the doped film. The Er,Yb: ZnO/Si film was placed in a quartz dish and then mounted at the focal point of the excitation 980 nm light. The integrating sphere was mounted on the fluorimeter with the entry and output ports of the sphere located in 90 geometry from each other in the plane of the spectrometer. The QYs were measured with

the integrating sphere via synchronous scans of the excitation and emission mono-chromators. The error involved in the UC-QY measurements is 5% relative.

The QY was determined for all as-deposited and annealed ZnO:Er,Yb films. These measurements lead to the evaluation of the most efficient doping for the $^4I_{11/2}$ to $^4I_{15/2}$ emission. Figure 5a shows the QY percentages *vs* the power density of the annealed ZnO: 3 mol.% Er, 9 mol.% Yb thin film under 980 nm. We found that the observed trends of UV, green and red of all the annealed films are similar. Firstly, the total UC quantum yield of all as-deposited ZnO/Er,Yb films is relatively low, on the order of about 1-1.4%. Moreover, as presented in Figure 5b, the power density dependence upconversion emission intensity curve for all three emissions shows that the threshold of the saturation of the emission intensity is at 19.3±0.3 W/cm^2 for ZnO: 3mol.%Er, 9mol.%Yb, which is lower compared to 20±0.3 W/cm^2 for β-$NaYF_4$: 2%Er, 20%Yb nanoparticles.[27,28] On the other hand, when annealing is employed, the total quantum yields are increased. As summarized in Table 1, the total UC-QYs values are 5.21±0.1%, 5.38±0.1%, 5.59±0.1% and 5.49±0.1% for films having 6, 8, 9 and 10 mol.% Yb concentrations, respectively. It is to be noted that the highest value of total UC-QY is 5.59 ±0.1% for the annealed ZnO:3mol.%Er, 9mol.%Yb thin film under a power density of 19.3±0.3 W/cm^2. These results are very promising compared to those obtained for β-$NaYF_4$:2%Er^{3+},20%Yb^{3+} in the form of colloidal nanoparticles with UC-QY of 0.3±0.3%, and the same sample in the bulk form with UC-QY of 3.0±0.1% under 20 W/cm^2.[27] It is mentioned that 3mol.%Er, 9mol.%Yb is the optimized Er/Yb concentration to get the higher absolute UC-QY for red (3.52±0.12%), green (1.76±0.10%), and UV (0.31±0.03%) emissions at the threshold excitation power density of 19.3±0.3 W/cm^2. It is reported in the literature that the power density of 20.3 W/cm^2 is well known to be the saturation regime of the power dependence curve.[27,35] The saturation of UC emission intensities beyond the excitation power

densities of 19.3±0.3 W/cm^2 in these measurements is in good agreement with the literature, which makes the film as a potential candidate for many photonic applications.[10,11,28]

It is concluded that the QYs of our ZnO:Er,Yb thin films exhibit extremely strong temperature dependence. Indeed, the as-deposited films show quantum yields of [1-1.4%] which they increased with almost three orders of magnitude to [5.21-5.59%] when the films were annealed at high temperature. These findings are in good accordance with the UC emission responses discussed above, which highlight the necessity of high temperature processing when trying to achieve upconverters with high luminescence efficiency. In addition, our results are similar to those of Er,Yb ions codoped $NaYF_4$ nanoparticles investigated by Faulkner et al.[36] In a deep study, the authors explained that the highest QY of red upconverted emission of hexagonal phased $NaYF_4$:Er,Yb structure is in extreme dependence with high temperature processing. Moreover, they elucidated that the removal of the defect structure in the materials with high temperature is the origin of the obtained results. Furthermore, in our QY measurements, the variation in the threshold excitation power density is low (19.3 to 19.6 W/cm^2) within the experimental error in the excitation power densities of 0.3 W/cm^2. It is reported that almost the same or even higher UC-QY can be achieved at the expense of higher excitation power density even at the lower concentrations of Yb^{3+}. This is can be originated from the difference in population path of each emitting state at different doping levels and at different excitation power densities. This aspect has also been proved in Yb^{3+}/Er^{3+} co-doped β-$NaYF_4$ nanoparticles[28] and phosphate glasses[37] materials.

Table 1. UC-QYs measured for annealed ZnO:Er,Yb films with different concentrations of Yb^{3+} at their corresponding threshold excitation power densities.

QY(%)	UV (410 nm)	Green (540 nm)	Red (665 nm)	Total QY(%)
ZnO:3mol.Er, 6mol.% at 19.4 W/cm^2	0.26±0.02%	1.57±0.1%	3.38±0.2%	5.21±0.1%
ZnO:3mol.Er, 8mol.% at 19.3 W/cm^2	0.31±0.04%	1.68±0.1%	3.39±0.1%	5.38±0.1%
ZnO:3mol.Er, 9mol.% at 19.3 W/cm^2	0.31±0.03%	1.76±0.1%	3.52±0.1%	5.59±0.1%
ZnO:3mol.Er, 10mol.% at 19.6 W/cm^2	0.28±0.02%	1.53±0.1%	3.68±0.2%	5.49±0.1%

It is well known that the decrease of upconversion quantum yield beyond the threshold of the excitation power density is originated from the saturation of the emitting states. This is due to the non-linear process of the UC emission process, which is highly dependent on the power density of the excitation 980 nm laser.

To understand the ZnO:3mol.%Er,9mol.%Yb UC mechanism, the pump power dependence of the upconverted UV, green and red emissions intensities were investigated in details in Figure 5c. For an unsaturated upconversion process, the emission intensity induced by irradiation with 980 nm laser is well described by power law: [38]

$$I \alpha P^n$$

where I is the integrated radiative intensity, P is the pump laser power, and *n* is the number of required laser photons. To determine the pump power dependence of the UC-QY, various ND filters in the 980 nm excitation beam were used. The excitation slit width was used to define the area and was kept constant at 20 nm. This ensured that the beam area (square) is same for all the measurements. The beam size was measured using an IR imaging camera (Electrophysics MicronViewer 7290A) and a beam diagnostic software. A total of 238 camera shots were taken and the average beam size was determined as $8x10^{-4}$ cm^2 with a relative error of 0.05%. The beam power was measured by a calibrated germanium photodiode

(Newport 818-IR) positioned at the focus of the excitation spot with a 1 μm resolution XYZ stage. The calibration error of the photodiode detector is ±4%. The combined error of calibration (of the photodetector) and uncertainty associated with the power density (in measured power meter readings and the measured area) measurement is ±4.2%.

It is noted that the number of pumping photons *n* can be evaluated from the slope of the UC intensity versus the laser excitation power in a log–log plot. The *n* values of the ZnO:3%.mol Er, 9 %.mol Yb thin films are found to be 1.91±0.2, 1.98±0.03 and 2.09±0.03 for the UV, green and red emissions, respectively. These results show that the UC mechanism is mainly happening due to a two-photon process which is mainly responsible for the upconverted emissions. The obtained results are in good agreement with those observed in other Yb^{3+}/Er^{3+} codoped $PbTiO_3$ ceramics.[34]

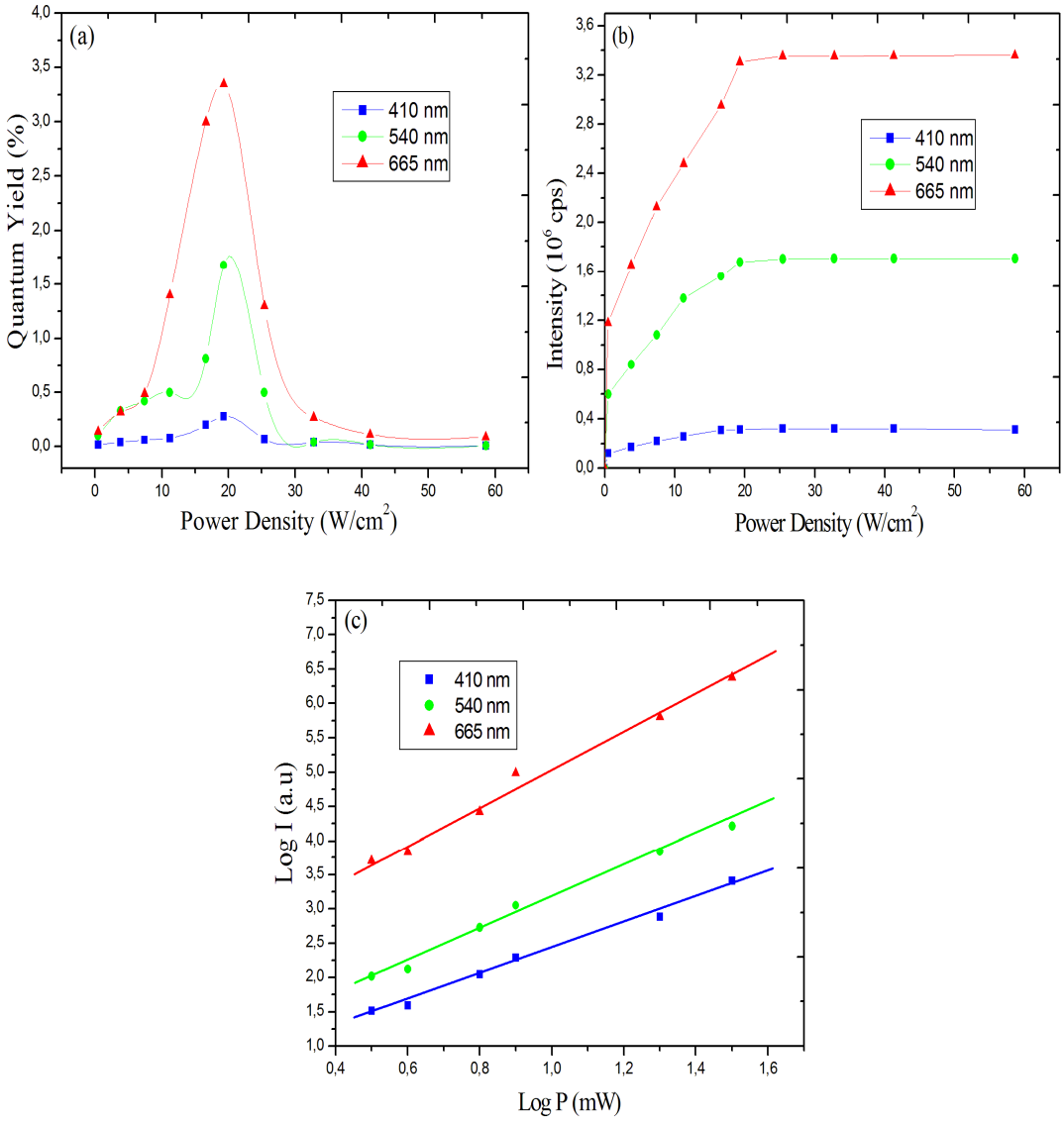

Figure 5. (a) Upconversion QY (%) variation with excitation power density, (b) Upconversion intensity variations with excitation power density and (c) double logarithmic plot of I as a function of power 980 nm laser for ZnO: 3mol.%Er^{3+}, 9mol.%Yb^{3+} upconversion emissions centered at 410, 540 and 665.

4. CONCLUSION

This study presents the potential of the ZnO/Er,Yb thin films with high efficient NIR→Visible upconversion emissions. The hexagonal phased structure films were successfully deposited by liquid source AACVD atmospheric pressure method. The optimized ZnO: 3%.mol Er and 9%.mol Yb films annealed at 1000°C was found to possess the strongest red emission (665 nm) than the other films. The obtained UC emissions was provided by two photon processes from the efficient Er/Yb energy transfer process governed by two mechanisms of $^4I_{15/2}$ (Er) + $^2F_{5/2}$ (Yb) →$^4I_{11/2}$ (Er) + $^2F_{7/2}$ (Yb) and $^4G_{11/2}$ (Er) + $^2F_{7/2}$ (Yb) → $^4F_{9/2}$ (Er) + $^2F_{5/2}$ (Yb). This optimized film showed a highest total UC-QY of 5.59±0.1% under a power density of 19.3±3 W/cm^2. Based on the present findings, the method we outline here is supposed to work for depositing ZnO:Yb^{3+}/Er^{3+} thin films as a highly efficient upconversion layer suitable for many photonic applications.

References

1 C. Wang, K. Song, Y. Feng, D. Yin, J. Ouyang, B. Liu, X. Cao, L. Zhang, Y. Hana and M. Wu, *RSC Adv*., 2014, **4**, 39118-39125.

2 E. Downing, L. Hesselink, J. Ralston and R. Macfarlane, *Science*, 1996, **273**, 1185-1189.

3 J. Wild, J. K. Rath, A. Meijerink, W. G. J. H. M. van Sark and R. E. I. Schropp, *Sol. Energy Mater. Sol. Cells*, 2010, **94**, 2395-2398.

4 M. Nyk, R. Kumar, T. Y. Ohulchanskyy, E. J. Bergey and P. N. Prasad, *Nano Lett*., 2008, **8**, 3834-3838.

5 X. J. Xie and X. G. Liu, *Nat. Mater*., 2012, **11**, 842-843.

6 P. A. Ma, H. H. Xiao, X. X. Li, C. X. Li, Y. L. Dai, Z. Y. Cheng, X. B. Jing and J. Lin, *Adv. Mater*., 2013, **25**, 4898-4905.

7 L. Li, C. Guo, S. Jiang, D. K. Agrawal and T. Lia. *RSC Adv*., 2014, **4**, 6391-6396.

8 M. Pang, X. Zhai, J. Feng, S. Song, R. Deng, Z. Wang, S. Yao, X. Gea and H. Zhang, *Dalton. Trans*., 2014, **43**, 10202-10207.

9 A. Shalav, B. S. Richards, T. Trupke, K. W. Krämer and H. U. Güdel, *Appl. Phys. Lett*., 2005, **86**, 013505-3.

10 H. P. Ho, W. W. Wong and S. Y. Wu, *Opt. Eng*., 2003, **42**, 2349-2353.

11 Q. H. Wang and M. Bass, *Electron. Lett*., 2004, **40**, 987-988.

12 G. Thomas, *Nature*, 1997, **389**, 907-908.

13 A. N. Banerjee and K. K. Chattopadhyay, *Prog. Cryst. Growth Charact. Mater*., 2005, **50**, 52-105.

14 T. Minemoto, T. Mizuta, H. Takakura and Y. Hamakawa, *Sol. Energy Mater. Sol. Cells*, 2007, **91**, 191-194.

15 Y. Chen, D. Bagnall and T. Yao, *Mater. Sci. Eng. B*, 2000, **75**, 190-198.

16 S. D. Ponja, S. Sathasivam, I. P. Parkin and C. J. Carmalt, *RSC Adv*., 2014, **4**, 49723-49728.

17 R. Elleuch, R. Salhi, N. Maalej, J. L. Deschanvres and R. Maalej, *Mater. Sci. Eng. B,* 2013, **178**, 1124-1129.

18 N. Khichar, S. Bishnoi and S. Chawla, *RSC Adv*., 2014, **4**, 18811-18817.

19 E. Alves, E. Rita, U. Wahl, J. G. Correia, T. Monteiro, J. Soares and C. Boemare, *Nuclear Instrum. Meth. Phys. Res. Sec. B*, 2003, **206**, 1047-1051.

20 H. Song and Y. J. Kim, *J. Europ. Ceram. Soc.,* 2007, **27**, 3745-3748.

21 J. M. Zhang and X. M. Feng, *Mater. Lett.,* 2008, **62**, 3224-3227.

22 T. Thomas, C. S. Blackman, I. P. Parkin and C. J. Carmalt, *Dalton Trans*., 2011, **40**, 10664-10669.

23 S. Basharat, C. J. Carmalt, R. Binions, R. Palgrave and I. P. Parkin, *Dalton Trans*., 2008, **5**, 591-595.

24 M. P. Hehlen, N. J. Cockroft, T. R. Gosnell and A. J. Bruce, *Phys. Rev. B*, 1997, **56**, 9302-9318.

25 G. S. Yi and G. M. Chow, *Chem. Mater*., 2007, **19**, 341-343.

26 T. Kano, H. Yamamoto and Y. Otomo, *J. Electrochem. Soc*., 1972, **119**, 1561-1564.

27 J. C. Boyer and F. C. J. M. van Veggel, *Nanoscale*, 2010, **2**, 1417-1419.

28 M. Pokhrel, A. k. Gangadharan and D. K. Sardar, *Mater. Lett*., 2013, **99**, 86-89.

29 R. Elleuch, R. Salhi, S. I. Al-Quraishi, J. L. Deschanvres and R. Maâlej, *Phys. Lett. A*, 2014, **378**, 1733-1738.

30 R. Elleuch, R. Salhi, J. L. Deschanvres and R. Maalej, *J. Appl. Phys*., 2015, **117**, 055301.

31 M. Ishii and Y. Komukai, *Appl . Phys. Lett*., 2001, **79**, 934-936.

32 F. Vetrone, J. C. Boyer, J. A. Capobianco, A. Speghini and M. Bettinelli, *J. .Appl. Phys.,* **96**, 661-667.

33 G. M. Salley, R. Valiente and H. U. Gudel, *J. Lumin*., 2001, **94**, 305-309.

34 F. C. D. Lemosa, D. M. A. Meloa and J. E. C. da Silva, *Mater. Res. Bull*., 2005, **40**, 187-192.

35 J. C. de Mello, H. F. Wittmann and R. H. Friend, *Adv. Mater.* 1997, **9**, 230–232.

36 D. O. Faulkner, S. Petrov, D. D. Perovic, N. P. Kheranib and A. O. Geoffrey , *J. Mater. Chem*., 2012, **22**, 24330–24334.

37 H. Desirena, E. De la Rosa, L. A. Diaz-Torres and G. A. Kumar, *Opt. Mater*., 2006, **28**, 560-568.

38 M. Pollnau, D. R. Gamelin, S. R. Lüthi, H. U. Güdel, *Phys. Rev. B*, 2000, **61**, 3337-3346.

Graphical Abstract

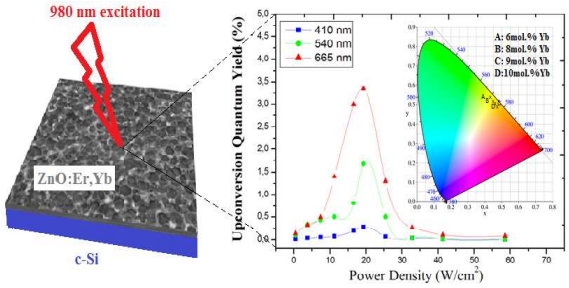

ZnO:Er,Yb hexagonal wurtzite phased structure thin film with high efficient NIR to visible upconversion emissions